Range Errors in Wind Profiling Caused by Strong Reflectivity Gradients

PAUL E. JOHNSTON AND LESLIE M. HARTTEN

Cooperative Institute for Research in Environmental Science, University of Colorado, and NOAA/Aeronomy Laboratory, Boulder, Colorado

CARL H. LOVE AND DAVID A. CARTER

NOAA/Aeronomy Laboratory, Boulder, Colorado

KENNETH S. GAGE

NOAA/Aeronomy Laboratory, and Cooperative Institute for Research in Environmental Science, University of Colorado, Boulder, Colorado

(Manuscript received 25 June 2001, in final form 7 November 2001)

ABSTRACT

Comparisons of data taken by collocated Doppler wind profilers using 100-, 500-, and 1000-m pulse lengths show that the velocity profiles obtained with the longer pulses are displaced in height from contemporaneous profiles measured with the shorter pulses. These differences are larger than can be expected from random measurement errors. In addition, there is evidence that the 500-m pulse may underestimate the wind speed when compared with the 100-m pulse.

The standard radar equation does not adequately account for the conditions under which observations are made. In particular, it assumes that atmospheric reflectivity is constant throughout the pulse volume and that observations can be assigned to the peak of the range-weighting function. However, observations from several tropical profilers show that reflectivity gradients with magnitudes greater than 10 dB km^{-1} are common. Here, a more general radar equation is used to simulate the radar response to the atmosphere. The simulation shows that atmospheric reflectivity gradients cause errors in the range placement. Observed reflectivity gradients can be used to calculate a correction to the range location of the observations that helps to reduce these errors.

Examples of these errors and the application of the correction to selected cases are shown. The evidence presented shows that reflectivity gradients are the main cause of the pervasive differences observed between the different radar observations.

1. Introduction

Radars have been used to measure vertical profiles of wind since the late 1960s; Van Zandt (2000) gives an overview of the history of wind-profiling radars. Several networks of wind profilers are now collecting data. The National Oceanic and Atmospheric Administration (NOAA) Profiler Network (NPN; Wuertz et al. 1995; Chadwick and Ackley 1997) in the central United States and the European Cooperation in the Field of Scientific and Technical Research (COST) Wind Initiative for a Network Demonstration in Europe (CWINDE; Oakley et al. 2000) network in Europe were both designed to provide frequent wind profiles to operational NWP centers. The NOAA Trans-Pacific Profiler Network (TPPN; Gage et al. 1990; Johnston et al. 1997) was designed primarily for climate research over the tropical Pacific basin, although much of its data are also used operationally.

Both UHF and VHF radars are used for wind profiling; operational details are found in Carter et al. (1995) and Gage et al. (1994). The UHF profilers in particular are often operated in two or more different modes, each using a different pulse length; this yields improved coverage over a deeper portion of the atmosphere. In some cases (e.g., at Piura, Peru; Biak, Indonesia; and Christmas Island, Kiribati, in the TPPN), multiple radars are collocated. With all these radars, the winds measured at each level represent a reflectivity-weighted average over the pulse volume of the radar beam. The winds are assigned to a fixed height calculated from the range that corresponds to the center of the radar's response to a point target in space (Doviak and Zrnić 1993, their section 4.4.3). This range assignment depends on the transmitted waveform and the radar receiver frequency response, and is independent of atmospheric conditions.

Corresponding author address: Paul E. Johnston, NOAA/Aeronomy Laboratory, R/AL3, 325 Broadway, Boulder, CO 80305-3328.
E-mail: Paul.E.Johnston@noaa.gov

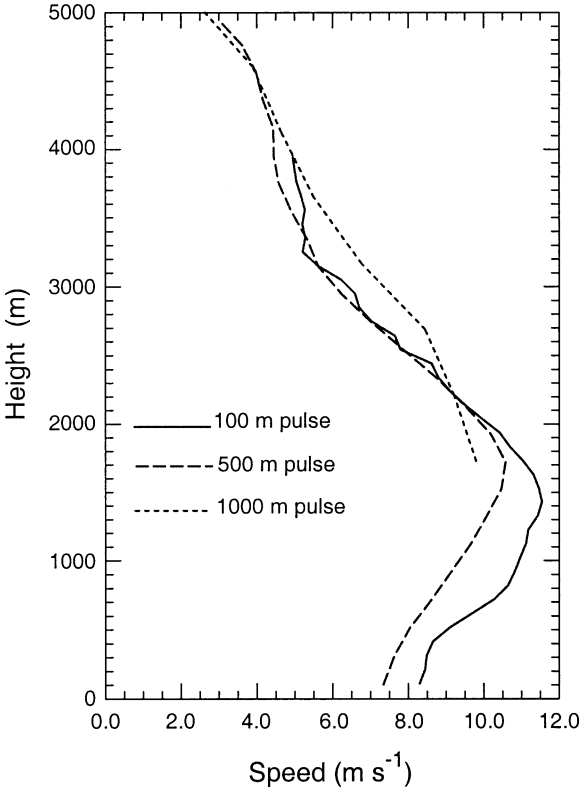

FIG. 1. Long-term mean profiles of wind speed measured at Christmas Island. The 100- and 500-m pulse length data are from the 915-MHz profiler. The 1000-m pulse length data are from the 50-MHz profiler. The profiles are mean values for Feb 1994, 1995, and 1996, constructed from a common set of daily means.

Comparisons of velocity profiles measured with different frequencies and pulse lengths show differences that cannot be explained as simple calibration errors. These differences are observed at many different locations and in data averaged over many different timescales, from individual 30-s radial velocity profiles to seasonal and annual averages. These differences are larger than can be expected from random noise and seem systematic. One example is shown in Fig. 1, using data from two collocated wind profilers on Christmas Island (2°N, 157°W). A common set of daily mean profiles from February 1994, 1995, and 1996 was used to construct the long-term mean. Below 2 km, the 500-m 915-MHz profile appears to have a consistent height offset when compared with the 100-m 915-MHz winds; note especially the location of the speed maximum. The 1000-m wind profile is much smoother than the 100-m one because of the larger volume being integrated for each observation, and appears to be offset in height from the 915-MHz profiles. Similar discrepancies have been seen at other TPPN sites (cf. Hartten and Gage 2000, their Fig. 1), as well as in data collected at Saipan, Northern Mariana Islands (15.11°N, 145.72°E) and Darwin, Australia (12.44°S, 130.95°E) (P. T. May 2001, personal communication).

One possible source of this type of error could be an incorrect calibration of the range for the radar. However, different calibrations of the TPPN radars show that calibration errors do not account for these discrepancies. These calibrations have been done using different measurement techniques and show that the range calibrations are stable and repeatable. Another potential source of these differences is gradients of reflectivity in the atmosphere. Range errors caused by gradients in reflectivity have been shown to be one source of a bias in the temperature measurements made with a radio acoustic sounding system (RASS) using UHF profilers (Angevine and Ecklund 1994; Görsdorf and Lehmann 2000). Expecting these errors to also exist in the wind measurements is reasonable. As an illustration, consider a 1000-m pulse in a region of the atmosphere where the reflectivity falls off 5 dB km^{-1}. In one pulse volume, the reflectivity will decrease by a factor of 3, biasing the results to the bottom of the pulse volume.

Velocity measurement errors caused by reflectivity gradients interacting with finite dimension antenna beamwidths have been examined by other researchers. Sloss and Atlas (1968) reported on spectral broadening caused by wind shear and reflectivity gradients. Fukao et al. (1988) reported on velocity measurement errors caused by thin atmospheric layers. However, both papers discussed velocity measurement errors, not range assignment errors caused by reflectivity gradients along the radar pointing direction. Green et al. (1979) present an example of a velocity observation that appears to be biased toward the velocity at lower heights by large reflectivity gradients. They characterize the bias as a velocity error, not as a range assignment error as proposed in this paper.

This paper explores the effects of atmospheric reflectivity gradients on retrieved wind profiles. Section 2 presents observations of tropical reflectivity gradients made by TPPN profilers. Details of the radar equation are given in section 3. Results of a simulation of the radar equation are shown in section 4. Section 5 contains the development of our range correction technique. This range correction method, which is applied to some radar data, is presented in section 6. Section 7 combines 100-m pulse length observations with the simulation in order to validate the simulation and predict radar observations for other pulse lengths. Section 8 contains a discussion of the results and future plans. Conclusions are given in section 9.

2. Observations of reflectivity gradients

Before examining the theory explaining the radar response to gradients of reflectivity, it is important to show that substantial gradients exist. This section presents some data describing the size and distribution of the reflectivity gradients. The important result that will be shown in this section is that large reflectivity gradients are frequently observed.

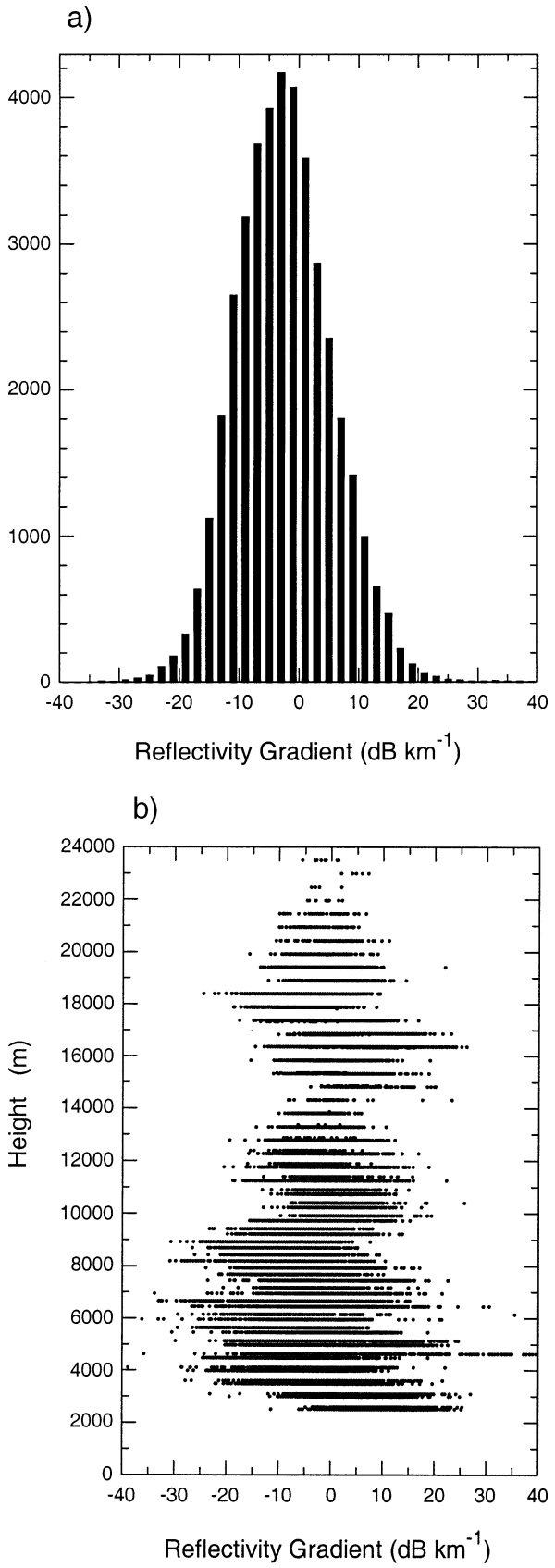

Many different studies of the variations of the refractive index structure parameter, C_n^2, have been conducted. Doviak and Zrnić (1993, their section 11.6.1) present several of these results. One simple form for the median value for C_n^2 comes from forward radio transmission measurements made by the U.S. National Bureau of Standards (NBS) (Doviak and Zrnić 1993; see their Fig. 11.17 and accompanying text). The gradient of this median C_n^2 is -2.17 dB km^{-1} and applies to the entire troposphere.

Wind profilers are usually not well calibrated in absolute reflectivity, but their relative reflectivity measurements are quite good (Gage et al. 2000). We have developed a simple three-step procedure for the calculation of the gradients of reflectivity. First, the relative reflectivity at each height is computed by multiplying the received-power values by the square of the range. Second, the relative reflectivities were then converted to a logarithmic scale, decibels. Third, the difference between the successive relative reflectivities (in dB) was then divided by the radial distance between the samples to get the reflectivity gradients. The reflectivity gradients are only calculated between successive heights. Only received power values more than 2 dB above the noise floor are used.

Figure 2 shows reflectivity gradients measured with the Christmas Island 50-MHz wind profiler. (The latitude and longitude of all TPPN profilers discussed in this paper appear in Table 1.) Data from one vertical and four oblique antenna beams collected on 20 and 21 October 1999 using a 1-km-long pulse are included. Observations below 2100 m have been excluded because of instrument recovery artifacts in the measured received power. The radar samples at constant ranges, so the vertical data appear in these scatterplots slightly above data from the oblique beams. The vertical-beam data may be due to both Bragg scatter and specular reflections from stable layers. The radar equation makes no distinction as to the type of scatter mechanism, so no attempt has been made to limit the discussion to one type of echo. Figure 2a shows a histogram of the reflectivity gradients measured, while Fig. 2b shows the same data plotted as a function of height above the radar.

Figure 3 shows a similar analysis of data from the Tarawa, Kiribati, 915-MHz wind profiler on 4 and 5 June 2000. Data are from two oblique beams and one vertical antenna beam, using a 100-m pulse. In Fig. 3, data below 450 m have been omitted, since the nonlinear response of the radar in this region causes high gradients that are instrumental and not atmospheric in nature. All

←

FIG. 2. Gradients of reflectivity measured with the Christmas Island 50-MHz wind profiler using a 1000-m pulse length on 20 and 21 Oct 1999. Data from one vertical and four oblique antenna beams are combined in these plots. The gradients are shown (a) in a histogram, where bin size = 2 dB km^{-1}, and (b) as a function of height above the radar.

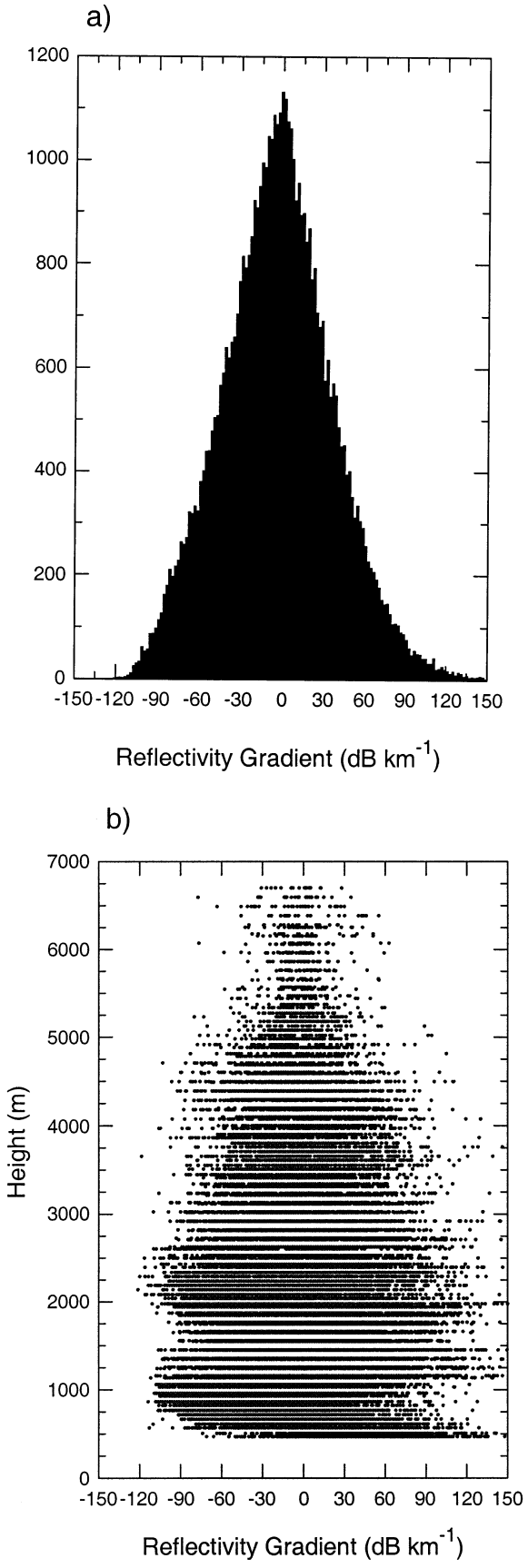

data used in Figs. 2 and 3 have been manually checked to remove most nonatmospheric returns.

The histograms (Figs. 2a and 3a) show distributions that are offset toward the -2.17 dB km^{-1} value of the median C_n^2 profile discussed above. Figures 2b and 3b show that a wide range of gradients occurs at all heights. The 1000-m pulse length used in the 50-MHz system observes a larger volume in space and smooths out any large reflectivity gradients caused by thin atmospheric layers. This causes the longer pulses to report smaller values of the gradient than the 500- and 100-m pulses used in the 915-MHz system.

We have looked at data from wind profilers in other locations and find very similar results, indicating that the data in Figs. 2 and 3 are typical of what is observed with wind-profiling radars. Table 1 shows results from several different radars deployed across the Pacific Ocean. The data cover randomly selected 1- or 2-day periods. The data from the radars in Biak, Nauru, and the Galápagos Islands have not been edited for nonatmospheric values, although known instrumental effects have been removed. The data from Tarawa and Christmas Island have been edited to remove most nonatmospheric target contamination (sea clutter, ground clutter, birds, airplanes, etc.).

Table 1 shows that median reflectivity gradients found in these data are within 2 dB km^{-1} of the -2.17 dB km^{-1} median value observed by the NBS, suggesting that it is a representative value for reflectivity gradients in the atmosphere. The standard deviations are smallest for 1000-m pulse lengths and largest for data including 100-m pulse lengths. The last column of Table 1 contains the fraction of the reflectivity-gradient population that is within two standard deviations of the arithmetic mean. Thus, less than 8% of the observed reflectivity gradients lie in the tails of the distributions. Spot checks, at each site, of several hundred of the values in the center of the distributions show that they are from atmospheric returns.

It is not the intent of this paper to present a detailed study of reflectivity gradients in the atmosphere, but rather to explain the effects of these gradients on the measurements and how they are interpreted. While there are differences between the reflectivity gradients observed with the different radars, sizeable gradients are clearly observed with all systems.

3. Radar equation

A version of the radar equation commonly used for wind-profiling radars is Doviak and Zrnić's (1993) Eq. (4.16):

←

FIG. 3. Gradients of reflectivity measured with the Tarawa 915-MHz wind profiler using a 100-m pulse length on 4 and 5 Jun 2000. Data are from one vertical and two oblique antenna beams. The gradients are shown (a) in a histogram, where bin size = 2 dB km^{-1}, and (b) as a function of height above the radar.

$$P(r_0) = \frac{P_t g^2 g_s c\tau\pi\theta_1^2\lambda^2}{(4\pi)^3 r_0^2 l_r 16\ \ln(2)}\frac{\eta(r_0)}{l(r_0)^2} = C\frac{\eta(r_0)}{l(r_0)^2 r_0^2}. \quad (1)$$

It states that the received power $P(r_0)$ at a given range from the radar r_0 is proportional to the reflectivity at that range $\eta(r_0)$, the attenuation over the path to that range $l(r_0)$, and the inverse of the square of the range. The constant of proportionality is radar-dependent and includes the transmitted power P_t, the antenna gain g, the antenna beamwidth θ_1, the radar system gain g_s, the velocity of light c, the filter loss factor l_r, and the radar wavelength λ.

This radar equation relies on two main assumptions. First, the reflectivity $\eta(r_0)$ is constant over the scattering volume. Second, the range to the scattering volume r_0 is large with respect to the pulse length. Figures 2 and 3 show that the assumption of constant reflectivity throughout the pulse volume is probably not valid. The second assumption, that the range is much larger than the pulse volume, is sometimes not valid. The 1000-m pulse wind speed profile shown in Fig. 1 starts at 1730 m. In the Tarawa data in Table 1, some of the data obtained with 500-m pulses starts near 700 m.

A more general radar equation [after Doviak and Zrnić 1993, their Eq. (4.11)], such as

$$P(r_0) = \int_0^{r_2}\int_0^{\pi}\int_0^{2\pi}\eta(r)\frac{C_0 f^4(\theta,\phi)|W(r_0, r)|^2}{l^2(r)r^4}r^2\, dr\, \sin\theta\, d\theta\, d\phi, \quad (2)$$

could be used. Here, the received radar power $P(r_0)$ is the integration over the volume containing the transmitted pulse; the reflectivity depends on r and r_0; C_0 is a system constant that is radar-dependent and includes such things as the transmitted power, the receiver loss values, and the system gain; the antenna spatial response is $f(\theta, \phi)$; and $|W(r_0, r)|^2$ is the range-weighting function of the radar, controlled by the transmitted waveform and the receive frequency response.

The full radar equation (2) is a complex triple integral that is difficult to apply. The functions are complicated and sometimes not well defined. For this paper, we reduce the general equation to a single integral by assuming that the antenna beams are narrow enough to not be affected by the reflectivity gradients, thereby removing the angular variations of the antenna. We also assume that the antenna beams are circularly symmetric so we can use the Probert-Jones approximation (Probert-Jones 1962) for the antenna. Also, wind profilers work at low enough frequencies that the atmospheric path loss $l(r)$ is negligible, so the $l(r)$ term can be dropped. This allows us to write the radar equation as

$$P(r_0) = C_1\int_0^{r_0+\Delta r}\eta(r)\frac{|W(r_0, r)|^2}{r^2}\, dr, \quad (3)$$

where the integration is only in range. The range-weighting function is shown as $|W(r_0, r)|^2$ to indicate that the function is centered at the range r_0. The upper integration limit is chosen so that targets that have not been illuminated by the transmitted pulse cannot contribute to the received power at r_0.

The velocity observed by the radar is also weighted by the reflectivity of the scattering volume. Doviak and Zrnić (1993, p. 110) show that the velocity observed by this type of radar is the true atmospheric velocity $\nu(r)$ weighted by the reflectivity and range-weighting functions. While it takes much signal processing to get the velocity observed by the wind-profiling radars, an equation similar to (3) can be written to describe the observed velocity:

$$V_{\text{Observed}}(r_0) = \frac{C_2\int_0^{r_0+\Delta r}\nu(r)\eta(r)\frac{|W(r_0, r)|^2}{r^2}\, dr}{P(r_0)}. \quad (4)$$

TABLE 1. Reflectivity gradients observed at various TPPN sites. Gradients were computed from all available observations during one or two randomly selected days. Known instrumental effects have been removed from these datasets. No attempt has been made to screen out nonatmospheric echos (e.g., point targets) from the Biak, Nauru, and Galápagos data.

Site	Pulse length (m)	Number of points	Median (dB km^{-1})	Arithmetic mean (dB km^{-1})	Standard deviation σ (dB km^{-1})	Population within ± 2 σ of the mean (%)
Biak 50-MHz profiler (1.1°S, 136.1°E)	1000	35 944	−1.9	−1.6	6.7	95.4
Christmas Island 50 MHz profiler (2.0°N, 157.3°W)	1000	40 617	−2.8	−2.5	8.0	95.6
Tarawa 915-MHz profiler (1.4°N, 172.9°E)	500	23 146	−4.2	−3.1	9.0	96.3
Tarawa 915-MHz profiler	100	49 888	−3.5	−3.2	40.3	95.2
Nauru 915-MHz profiler (0.5°S, 166.9°E)	100 and 500	45 488	−0.8	−1.8	32.1	94.0
Galápagos 915-MHz profiler (0.9°S, 89.6°W)	100 and 500	23 376	−2.1	0.7	41.2	92.8

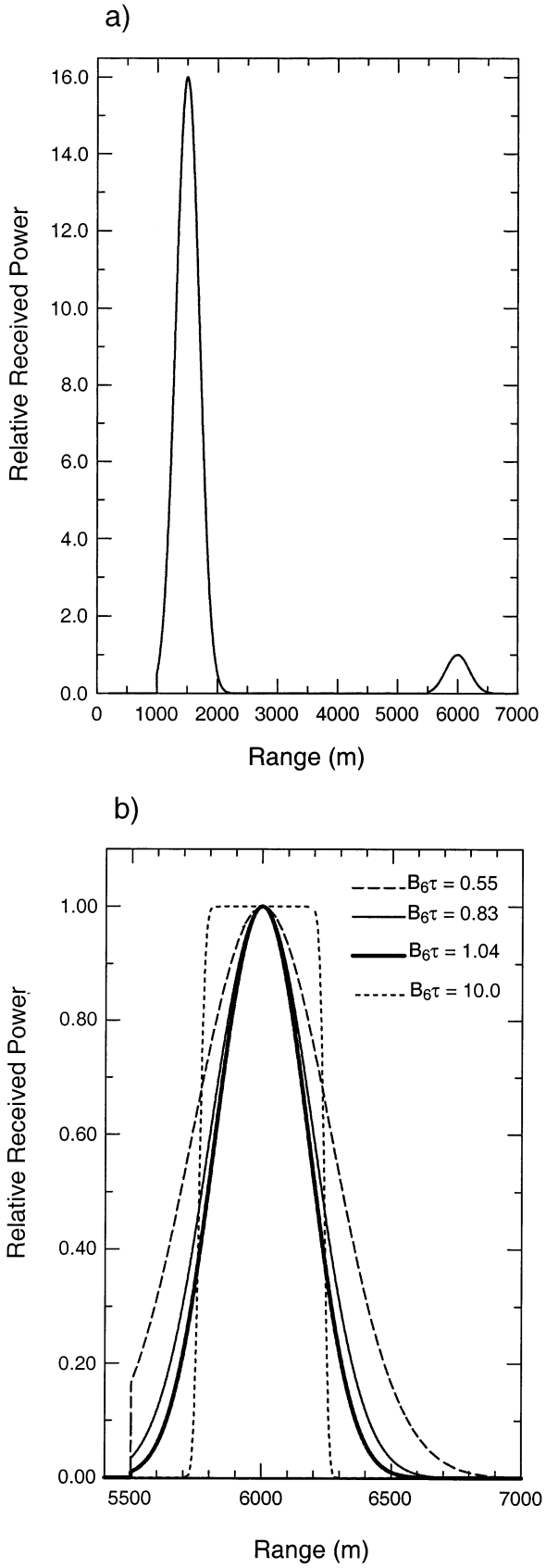

Note that in (4) the velocity integral is normalized by the received power, so it does not depend on the absolute reflectivity calibration of the radar.

Equations (3) and (4) both show that the received power and velocity values observed by the radar are related to the integrated values of the range-weighting function reflectivity product, $[\eta(r)\,|\,W(r_0, r)\,|^2]/r^2$. In the original radar equation formulation, the underlying assumptions cause the peak of this product to be at the center of the range-weighting function, $|\,W(r_0, r)\,|^2$, thus assigning the measurements to the range r_0. The power and velocity response of the radar system is the integration of the reflectivity weighted by the range-weighting function and a falloff with range. When there are gradients in the reflectivity, the received power and observed velocity can come from a range that is considerably different from r_0.

In most wind-profiling radars, the transmitted waveform is rectangular, and the receive filter function is approximately Gaussian. The range-weighting function can be shown to have the form

$$|W(r_0, r)|^2 = \left|\frac{1}{2}\left\{\operatorname{erf}\left[\frac{\pi(B_6\tau)}{2\sqrt{\ln 2}\,\mathrm{PW}}\left(r_0 - r + \frac{\mathrm{PW}}{2}\right)\right] - \operatorname{erf}\left[\frac{\pi(B_6\tau)}{2\sqrt{\ln 2}\,\mathrm{PW}}\left(r_0 - r - \frac{\mathrm{PW}}{2}\right)\right]\right\}\right|^2, \tag{5}$$

which comes from the convolution of the transmitted waveform and the receiver filter function [Doviak and Zrnić 1993, their section 4.4.3, especially Eq. (4.25)]. The term PW is the pulse length of the transmitted pulse (m). The factor $B_6\tau$ is the product of the half-voltage (-6 dB) frequency response of the radar receiver times the transmitted pulse duration (s) τ. It is a dimensionless quantity that is a good way to characterize radar response. Selection of the $B_6\tau$ to use in a radar system is a complex topic, since it involves trading off sensitivity for range resolution. A good compromise value of $B_6\tau$ is 1.04, the ''matched'' filter value, as discussed in Doviak and Zrnić (1993, p. 60).

4. Radar simulations

A radar simulation has been constructed using (3), (4), and (5) to simulate radar returns, including the velocity profile the radar will measure. The simulation starts at 20 m, to avoid the singularity at $r = 0$, and varies only along the radial direction. In this simulation

←

FIG. 4. Simulation of the power received from point targets using a 500-m-long pulse. (a) The response to two identical targets, one at 1500 m and one at 6000 m, using a $B_6\tau$ product of 0.83. (b) The power received from a point target located at 6000 m. Curves for $B_6\tau$ products of 0.55, 0.83, 1.04, and 10.0 are shown.

there are no system delays. This means that Δr in (3) and (4) is equal to the pulse length in space, PW $= c\tau/2$. Pulse length and $B_6\tau$ are used to describe the radar. Several options can be used to specify the reflectivity and velocity profiles used in the simulation. The program outputs the received power and velocity profiles for given profiles and radar parameters. It can output the integrands of (3) and (4). The first moment and standard deviation of the integrand of (3) are also calculated.

The first test of the simulation is its response to point targets. Figure 4a shows the simulation output for two point targets, one at 1500 m and the other at 6000 m. In this paper, measured radar data are presented with height (or range) along the vertical axis of the graph; simulated data are presented using the mathematical convention, with the independent variable (range) along the horizontal axis. For this simulation the pulse length was specified as 500 m, and the $B_6\tau$ product was set to 0.83, as is typical of some TPPN 915-MHz radars. In Fig. 4a, the received power has been normalized so that the peak power at 6000 m is 1.0. The sharp edge visible in the response to the target at 1500 m is caused by the upper limit of the integral in (3). The response to a pulse cannot start until the pulse reaches the target at 1500 m, but the range-weighting function is nonzero at 500 m from the target. The trailing edge of the target response is much longer, since the lower limit of the integral extends to zero range. The nonsymmetrical limits on the integration are important, since they imply that the radar can respond to targets far below r_0, but only to targets within a finite distance above r_0.

Some key points are evident in Fig. 4a. First, although the reflectivity profile consists of two point targets with no extent in range, the simulated profile has range extent, which arises from the range-weighting function. For point targets the radar response is proportional to $|W(r_0, r)|^2$. The peaks in Fig. 4a are images of the range-weighting function for a 500-m pulse length and a $B_6\tau$ product of 0.83. This function defines the region in space to which the radar is sensitive, therefore the range resolution of the radar. The definition of the range resolution used in this paper is the distance between the -6 dB values of the range-weighting function, which in this example is 648 m. This is equivalent to one conventional definition of range resolution as the distance between two point targets that will result in a -3 dB dip between the peaks of each target. Another commonly used definition of range resolution is the pulse length (500 m in this example).

Figure 4b shows the radar response of a 500-m-long pulse to a point target at 6000 m, using four different $B_6\tau$ products: 0.55, 0.83, 1.04, and 10.0. (Some TPPN radars are operated with $B_6\tau = 0.55$ or 0.83 values; $B_6\tau = 1.04$ is the ''matched'' filter value; and $B_6\tau = 10.0$ is an extreme value.) Figure 4b shows that the range resolution of a radar system is determined not only by the pulse length but also by the receiving system used to obtain the data. As the $B_6\tau$ product increases, the range resolution becomes equal to the pulse length. For the $B_6\tau = 0.55$ curve, the range resolution is 877 m. For the 0.83 curve it is 648 m, for 1.04 it is 574 m, and for $B_6\tau = 10.0$ it is 500 m. The range resolution, as determined by the -6 dB points of the range-weighting function, is important in determining how the reflectivity gradients affect the radar measurements. It is controlled by both the range-weighting function of the radar and the transmitted pulse length, not the distance between the range samples of the radar. The values of $B_6\tau$ used in the rest of this paper will be ones measured in the actual radar systems.

The second point that can be made from Fig. 4 regards the location of the targets. The received power in Fig. 4 is shown as a continuous function. In wind profilers, this function would be sampled at discrete points, typically spaced no farther apart than one pulse length. The targets are at 1500 and 6000 m in this simulation, but if sampling were done every 500 m, then there could be up to 250-m error in placement of the targets. This would happen when the samples were at 1250 and 1750 m (or 5750 and 6250 m), which would give equal power values. To reduce position errors, sampling the received power at spacing less than the resolution or pulse length is desirable.

The third point that can be made from the simulation shown in Fig. 4 is that the received power at 1500 m is 16 times that received at 6000 m. This is the ratio of the square of the ranges, and is predicted by (1). This leads to the first conclusion: for point targets (airplanes, birds, missiles, meteors, etc.), (1) is a good approximation and gives good reflectivity measurements, at least at these ranges.

For extended targets, the situation is more complicated. To study extended targets with the simulation, a reflectivity profile with a constant reflectivity gradient such as

$$\eta(r) = N_0 \exp\left\{\ln(10)\times\frac{M}{10\times1000}(r)\right\} \qquad (6)$$

is used. In this formulation the gradient M is expressed in the same units (dB km^{-1}) used for the actual data in section 2, and is specified in the simulation, as is the range at which the reflectivity is unity, which determines the value of N_0. Figure 5a shows, for a constant reflectivity gradient of -20 dB km^{-1}, the input reflectivity (solid line) and the simulated reflectivity (dashed line). The simulated reflectivity is simply the received power multiplied by the square of the range, normalized to be equal to the input reflectivity at 7000 m. The simulation is set for a 500-m pulse length and a $B_6\tau$ of 0.83, as in the first simulation.

Figure 5a shows that the reflectivity observed by a simulated radar at large ranges is proportional to the reflectivity that is input to the simulation. Figure 5b shows the difference between the simulated reflectivity

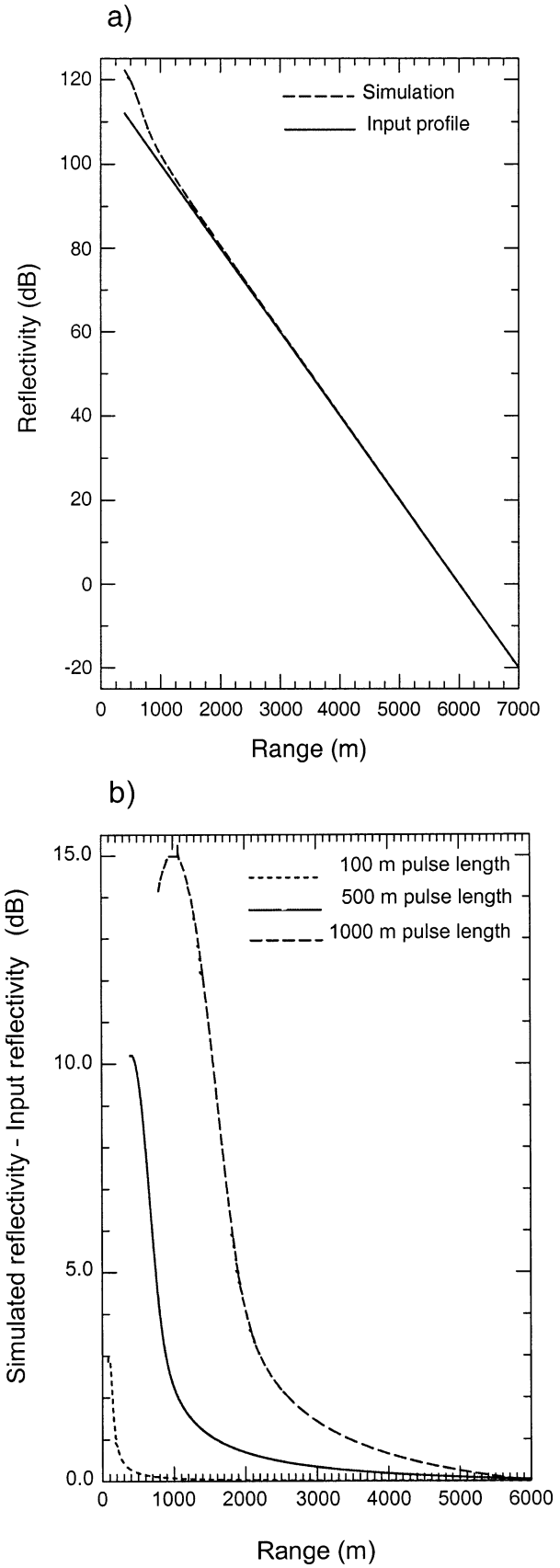

and the input reflectivity, as a function of the range from the radar. Curves for 100- and 1000-m pulse length simulations using the same $B_6\tau$ and reflectivity profiles are also plotted. Compared with the short pulse, the longer pulse lengths have more reflectivity change in the resolution volume and show a larger deviation from the input reflectivity profile. Close to the radar, the r^{-2} term of the integrand becomes important in the integration. This causes the radar response to become very nonlinear so that the differences between the linear radar equation (1) and the nonlinear radar equation (3) become quite large. As can be seen in Fig. 5b, the errors near the radar can be many decibels. For the extended target case, reflectivity measurements at ranges less than three pulse lengths should be viewed with caution.

Figure 6a shows the input velocity profile and the simulated velocity profile for a 500-m pulse length and a $B_6\tau$ of 0.83. This is the first clear example in this paper of the location error caused by a reflectivity gradient. The simulated velocity profile (dashed line) shows a definite range offset from the input velocity profile (solid line). For example, the input velocity profile has zero velocity at 6000 m. The simulated velocity profile has zero velocity at 6181 m, a range error of 181 m. Below 1000 m, the nonlinear effect caused by the r^{-2} term of (4) is evident.

Figure 6b highlights the region around 6000 m, where the input velocity profile is zero. The observed velocity when the reflectivity gradient is $+20$ dB km^{-1} (short dashed line) has been added to the plot. For these examples the range of the zero crossing varies from 5857 m (for $M = 20$ dB km^{-1}) to 6181 m (for $M = -20$ dB km^{-1}), or 324 m.

Reflectivity gradients will affect observations made with a long pulse length more than those made with a short pulse. In a noiseless world, we would only use short pulses and large $B_6\tau$ products and not be bothered by this effect. In the presence of noise, longer pulse lengths are more sensitive and capable of seeing higher into the atmosphere. The effects of pulse length are shown in Fig. 7, where simulations using three different pulse lengths (100, 500, and 1000 m) are shown. Each simulation used a reflectivity gradient of -20 dB km^{-1}. The input velocity profile is shown as the solid line and has zero velocity at 6000 m. The simulation with the 100-m pulse length ($B_6\tau = 0.83$) is barely visible, as it is only offset from the input velocity profile by 8 m. The 500-m pulse length simulation ($B_6\tau = 0.83$) has zero velocity that is

←

FIG. 5. The reflectivity estimated by a simulation using a 500-m-long pulse and a $B_6\tau$ product of 0.83 in an atmosphere with a -20 dB km^{-1} reflectivity gradient. (a) The input profile (solid line) and the simulation profile (dashed line). (b) The difference between the simulated reflectivity profile and the input reflectivity profile as a function of range (solid line). Difference curves for 100- and 1000-m-long pulses with the same reflectivity gradient and $B_6\tau$ product are also shown (dashed lines).

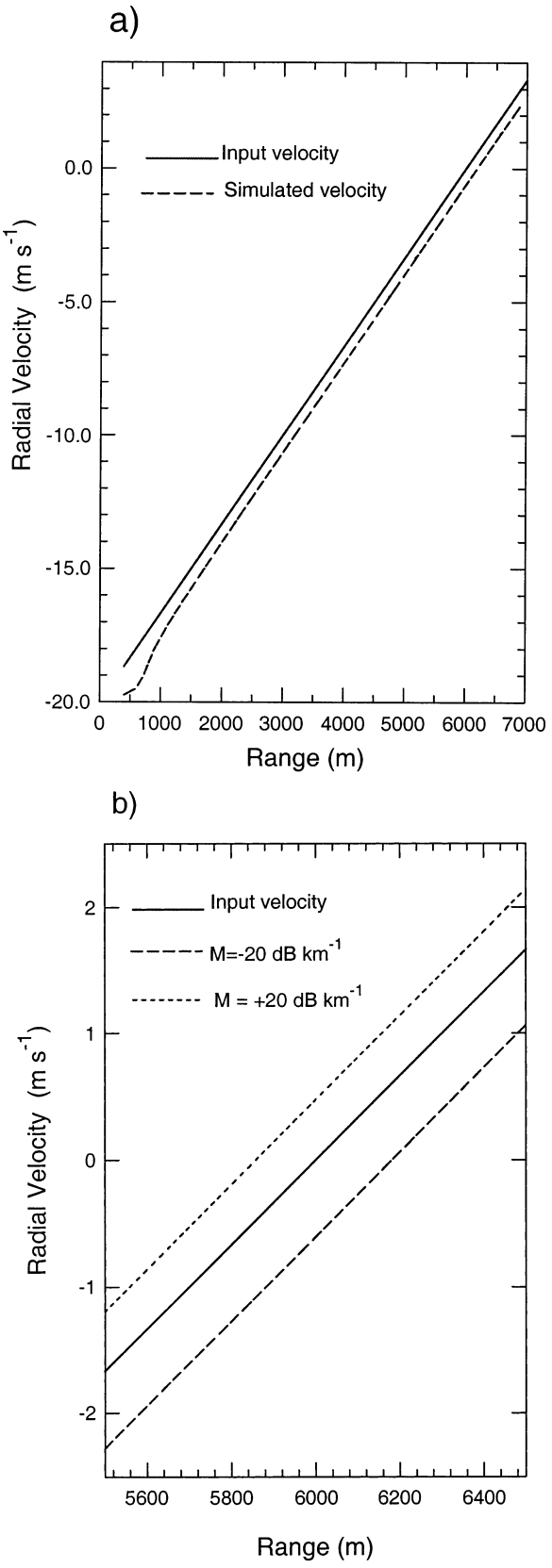

offset by 181 m, to 6181 m. The 1000-m pulse length simulation ($B_6\tau = 1.0$) has zero velocity at 6553 m, which is a 553-m offset, more than one-half of a pulse length.

To demonstrate the cause of this effect, we can use the output of the simulation to look at the integrand of the equations. Figure 8 shows the integrand of (3), $[\eta(r)|W(r_0, r)|^2]/r^2$, for three cases of reflectivity gradients: -20, 0, and $+20$ dB km^{-1}. In all cases, the range-weighting function is centered at 6000 m, and the integrand stops at 6500 m, the upper limit of the integration. This simulation is for a 500-m pulse length and a $B_6\tau$ of 0.83. The reflectivity is 1 at 6000 m, so the integrands are all equal at 6000 m.

Figure 8 shows the functions that are integrated to give the received power at 6000 m. In the -20 dB km^{-1} case, the integrand is weighted to ranges below 6000 m, since the reflectivity is decreasing with height. From the discussion of the range resolution that accompanied Fig. 4, we know that the range-weighting function, $|W(r_0, r)|^2$, peaks at 6000 m and drops off by 6 dB at 6000 $\pm$ 324 m (e.g., at 5676 and 6324 m). However, for this case, the reflectivity increases 6.48 dB between 6000 and 5676 m, so that the integrand is larger at 5676 m than at 6000 m. [For those not at ease with decibel values, 6.48 dB + (-6.0 dB) = 0.48 dB, or a factor of 1.12.] In a similar fashion, the reflectivity decreases above 6000 m, so that at 6324 m the integrand is down 12.48 dB instead of only 6 dB. This shifting of the response caused by the reflectivity gradient is shown as the -20 dB km^{-1} curve of Fig. 8.

In the $+20$ dB km^{-1} case, the reflectivity's increase with height displaces the integrand above 6000 m. In this case, the upper tail of the response is clearly stopped by the upper limit of the integration. Since this is caused by the location of the pulse in space, it means that the positive reflectivity gradient case is not shifted quite as much as the negative reflectivity gradient case.

All three of these simulations have the same integrand value at 6000 m, but after being integrated they do not give the same estimated reflectivity. The $M = -20$ dB km^{-1} case shows a reflectivity that is 4.6 dB above the reflectivity for the $M = 0.0$ dB case. The $M = 20$ dB km^{-1} case has a reflectivity that is 3.1 dB above the $M = 0.0$ dB km^{-1} value.

The atmospheric volume described by the radar measurements can be characterized by the range resolution and the first moment of the peak. Table 2 shows summary information for the curves in Fig. 8. The range

←

FIG. 6. The velocity estimated by a simulation using a 500-m-long pulse and a $B_6\tau$ product of 0.83 in an atmosphere with a -20 dB km^{-1} reflectivity gradient. (a) The input velocity profile (solid line) and the simulation results (dashed line). (b) The same simulation, confined to the range near 6000 m, where the velocities are near 0 m s^{-1}, together with an additional simulation in an atmosphere with a $+20$ dB km^{-1} reflectivity gradient.

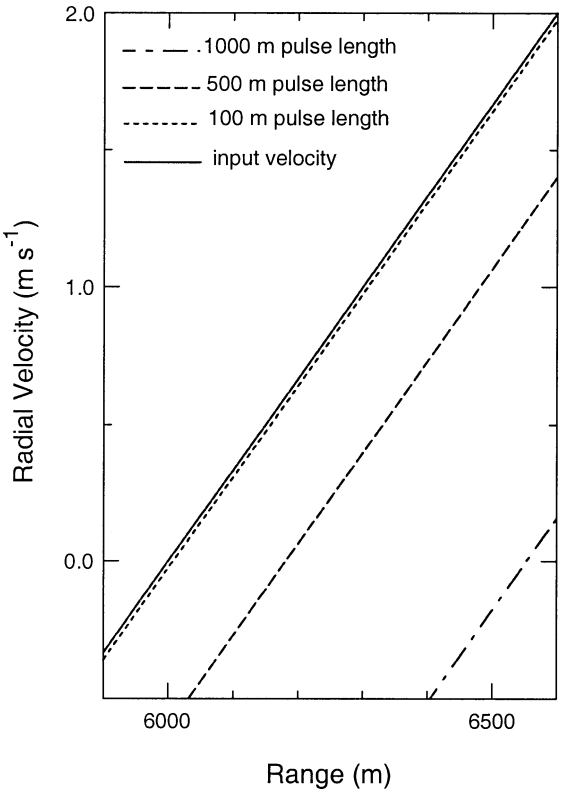

FIG. 7. Simulations of the velocity measured by a radar with 100-, 500-, and 1000-m-long pulses in an atmosphere with a -20 dB km^{-1} reflectivity gradient. Only the region around 6000 m, where the input velocity profiles are near 0 m s^{-1}, is shown.

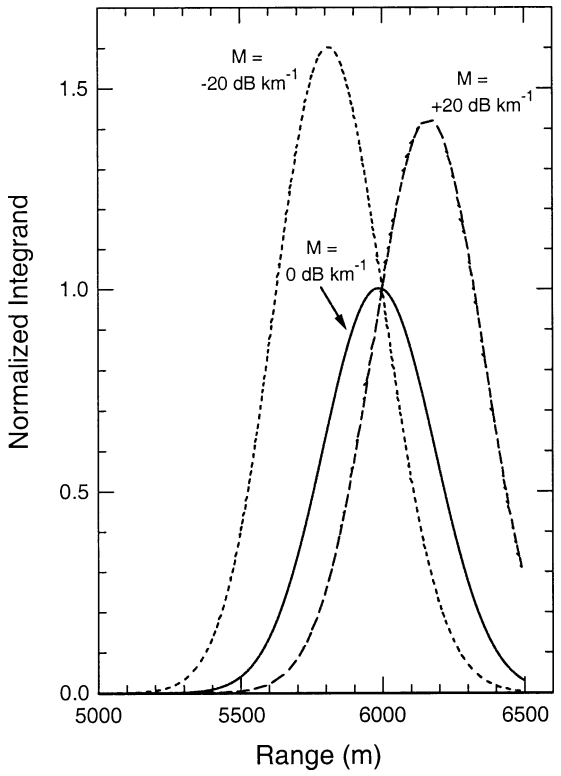

FIG. 8. Integrands of the received power from a simulation using a 500-m-long pulse and a $B_6\tau$ product of 0.83. Curves for an atmosphere with -20, 0, and $+20$ dB km^{-1} reflectivity gradients are shown. For all three curves, the range-weighting function was centered at 6000 m.

resolution, defined as the distance between the -6 dB points of the integrand, is insensitive to the reflectivity (but not the $B_6\tau$ product). The volume can shift considerably, depending on the local reflectivity, since the integrand remains nearly symmetrical about the peak but moves in range.

Figure 8 demonstrates the key point of this paper: *the peak of the range-weighting function is not an adequate description of the location of the echoing region when the reflectivity is not constant throughout the pulse volume.* In current wind profiler practice, these observations would be assumed to be from a 648-m-deep volume centered at a range of 6000 m. However, Table 2 shows that the first moments of the peaks vary in range from 5819 to 6143 m. This distance (324 m) is large with respect to the 500-m pulse length and can lead to velocity profile errors such as those shown in Green et al. (1979) and Figs. 1, 6, and 7.

5. Range correction technique

In an actual radar, we have access only to the integrated value of (3). Since this is a simulation, we are able to compute the first moment m_1 of each integrand. This represents the ''center of mass,'' or median of the integrand, and would be a logical range at which to place the data. By assuming that the local form of the reflectivity is that of (6), the integrand of (3) can be differentiated. The peak of the integrand r_1 can then be found by setting the derivative to zero and solving for r:

$$\frac{\sqrt{\pi}B_6\tau}{\sqrt{\ln(2)}\mathrm{PW}}\{e^{-B^2(r_0,r)} - e^{-A^2(r_0,r)}\} - \left\{\frac{1}{r} + \ln(10)*\frac{-M}{20*1000}\right\} \times \{\mathrm{erf}[A(r_0, r)] - \mathrm{erf}[B(r_0, r)]\} = 0$$

$$A(r_0, r) = \frac{\pi B_6\tau}{2\sqrt{\ln 2}}\left(r_0 - r + \frac{\mathrm{PW}}{2}\right)$$

$$B(r_0, r) = \frac{\pi B_6\tau}{2\sqrt{\ln 2}}\left(r_0 - r - \frac{\mathrm{PW}}{2}\right). \qquad (7)$$

This equation is not solvable in closed form. However, r_1 can be found by iteration, given the local reflectivity gradient M and the center of the range-weighting function r_0. The peak of the integrand r_1 can then be used instead of r_0 to place the data.

Figure 9 shows the offset from r_0 to both m_1 and r_1, for a 500-m pulse length and a $B_6\tau$ product of 0.83. Results

TABLE 2. Simulation results at 6000 m for different reflectivity models observed with a 500-m pulse length and a $B_6\tau$ product of 0.83.

Reflectivity model	Location of integrand peak (m)	Location of integrand first moment (m)	Lower −6 dB point (m)	Upper −6 dB point (m)	Range resolution (m)	r_0 (m)
−20 dB km^{-1}	5812	5819	5501	6137	636	6000
0 dB km^{-1}	5987	5986	5663	6312	649	6000
+20 dB km^{-1}	6164	6143	5838	6476	638	6000
Point target	6000	6000	5679	6324	645	6000

for reflectivity gradients of −20 and +20 dB km^{-1} are shown. For most ranges of interest, r_1 is farther from the center of the range-weighting function than m_1. Note that these offsets are a large fraction of a pulse length from the proper location. Also, these curves show again that at ranges less than about three pulse lengths, the r^{-2} term becomes increasingly important. Similar curves for other gradients and pulse lengths can be plotted, showing similar shapes but different offsets.

Figure 9 shows that choosing the peak of the integrand for the location of the measurement will overcompensate the range location error made by choosing the peak of the range-weighting function instead of the first moment of the integrand. In practice this should not be a problem when using the radar data to estimate the gradient of reflectivity. The Tarawa data in Table 1 show that in the same atmosphere, the long-pulse estimates of reflectivity are smaller than short-pulse ones. This means that the long-pulse estimated reflectivity gradients are underestimated, thereby negating the overcompensation of the integrand-peak-based correction.

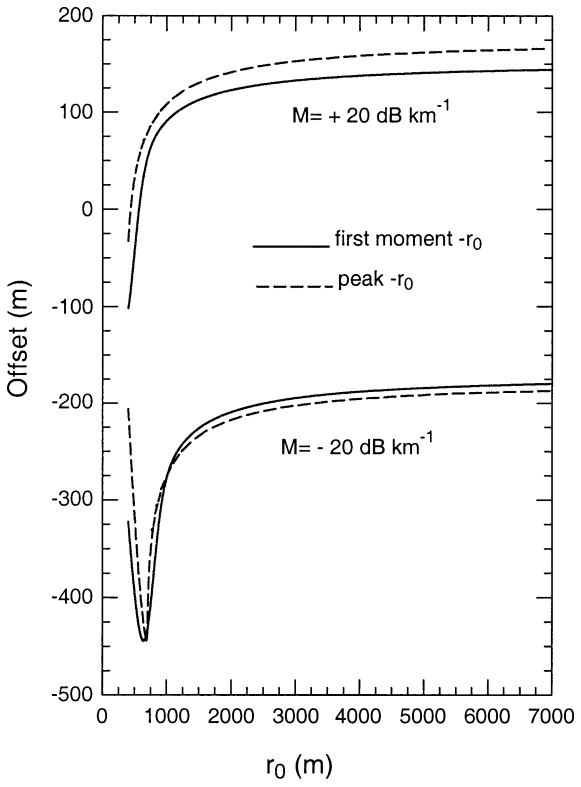

FIG. 9. Offsets of both the peak and the first moment of the integrand of received power from the center of the range-weighting function. These simulation results are for a 500-m-long pulse and a $B_6\tau$ product of 0.83 in an atmosphere with reflectivity gradients of −20 and +20 dB km^{-1}.

Our technique to correct the range of the measured data is to use the received power from the radar to estimate M, the gradient of the reflectivity. This value and the range of the center of the range-weighting function r_0 are input into (7), which is then solved by iteration for the peak of the integrand r_1. The measured radial data values (received power, velocity, spectral width, and noise level) are then assigned to r_1 instead of r_0. Since the range assignments of the data are changed, to use the data for multiprofile calculations such as wind vectors or time-averages, the data need to be interpolated back to constant range values. This interpolation is not done here; we limit the demonstration of the technique to radial components only.

6. Application to atmospheric observations

The first example of the application of this technique to radar data is shown in Fig. 10. Radial velocity profiles from the Christmas Island 50-MHz radar collected on 20 October 1999 are shown. These data are from an antenna beam with an azimuth of 270° and elevation angle of 75.7°. All of the profiles from 0000 to 0100 UTC are shown. Each successive profile has been offset by 2.0 m s^{-1} to separate the profiles on the plot. The solid lines are the observed profiles placed at the center of the range-weighting function, and the dashed lines are the profiles after the range correction has been applied.

Since we do not want to discard any reasonable velocity measurements, a constant correction has been applied to the lowest point of each profile, where there is no way to estimate the reflectivity gradient. This correction is determined using the NBS median atmospheric gradient of −2.17 dB km^{-1}. As mentioned in the discussion of Fig. 2, there is a problem with the received power measurement of the lowest gate caused by the radar electronics. This causes an erroneous M estimation for the second range, so the constant correction using $M = -2.17$ dB km^{-1} has also been applied to the data from this range. In the second, fourth, and last profiles (from the left), the data at 9700 m are missing, so the data at

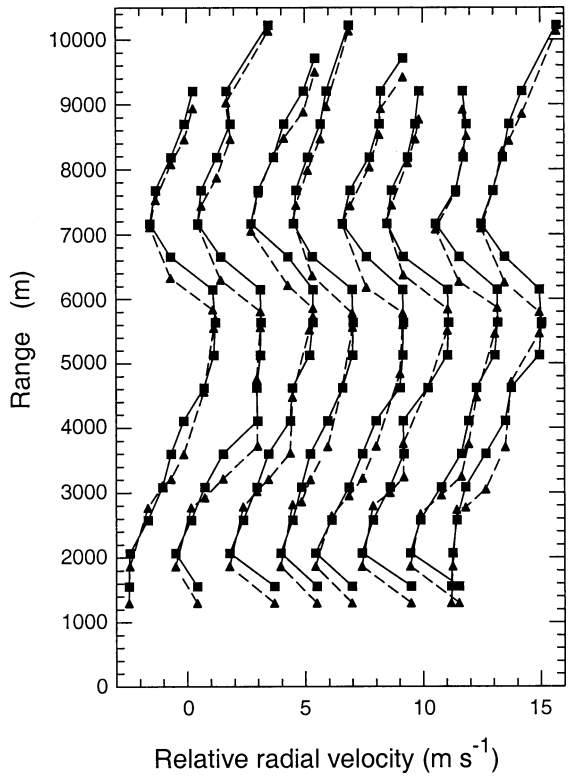

FIG. 10. Profiles of radial velocity measured with the Christmas Island 50-MHz wind profiler. The data are from the period 0000–0059 UTC 20 Oct 1999. Each successive profile has been offset by 2.0 m s^{-1} to provide separation on the plot. The solid lines place the velocity data at the center of the range-weighting function. The dashed lines place the velocity data at the peak of the integrand, based on the local reflectivity gradient measured by the radar.

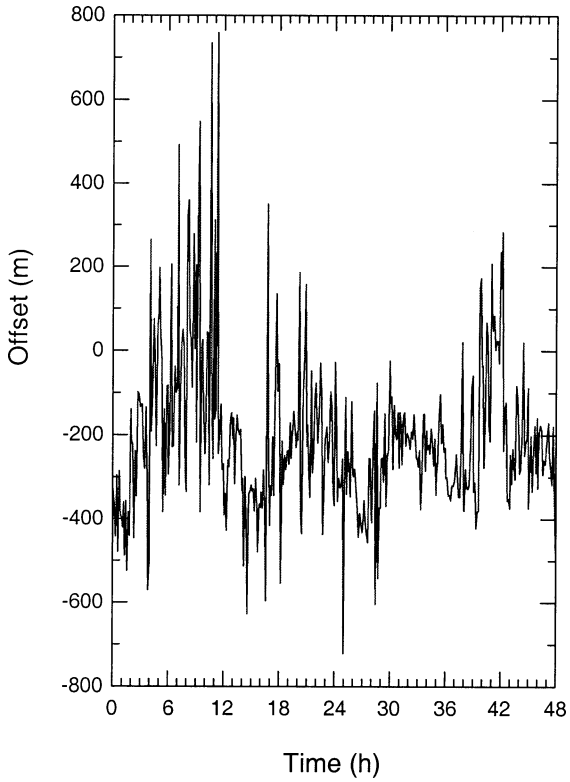

FIG. 11. The time series of the offset between the peak of the integrand and the center of the range-weighting function for the 6658-m range measured with the Christmas Island 50-MHz wind profiler. The time period shown covers 20 and 21 Oct 1999.

10 200 m have also been shifted using a -2.17 dB km^{-1} reflectivity gradient. From these data points that are corrected using $M = -2.17$ dB km^{-1} it can be seen that the correction is range-dependent, with the largest correction being made at the smallest ranges.

Could there be a constant range correction that would result in better velocity profiles without the trouble of correcting each profile? For example, could the mean reflectivity-gradient correction be used, arguing that over time the effects would average out to this value? Figure 2b, which includes the data shown in Fig. 10, shows that over the 2 days the gradients over Christmas Island vary considerably. Figure 11 shows the range correction to be applied to the data at 6452 m for the west beam of the Christmas Island 50-MHz radar on 20 and 21 October 1999. The median range correction for this hour is 204 m downward, with a standard deviation of 218 m. The profiles in Fig. 10 come from the first hour shown in Fig. 11, when the correction is around 400 m downward. Therefore, a constant correction at all heights does not seem justifiable. It is possible, however, that a constant profile of corrections could be developed. This set of corrections might be based on the average correction at each range over some suitable period, for example, a season or year. A climatology of the reflectivity gradients would need to be studied in order to be able to develop such a set of curves.

It was shown in Fig. 6b that the 100-m pulse length does not suffer from much range offset, so we have chosen not to apply the range corrections to the 100-m observations. Figure 12a shows velocity profiles from the Christmas Island 915-MHz radar. The 100-m data are from 1256:29 UTC 20 October 1999, and the 500-m data are from 1257:10 UTC. These are data from the antenna beam with an azimuth of 90° and elevation angle of 76.2°. The radial velocity at 330 m (in the 100-m profile) has been manually corrected, because the radar software selected the wrong spectral peak and reported the wrong value. The range of the lowest two 500-m data points was corrected using the median atmospheric gradient; the rest of the points were corrected using the reflectivity gradients calculated from the 500-m data. Clearly, the corrected profile more closely matches the 100-m profile. In particular, the velocity peak moved to ranges that more closely match the 100-m data, and the profile above the peak velocity is closer to the 100-m profile. Note that the data at 435 m dropped 237 m to a range of 198 m, while the point at 750 m dropped 116 m to 634 m, though they were both corrected with the median reflectivity gradient. This again

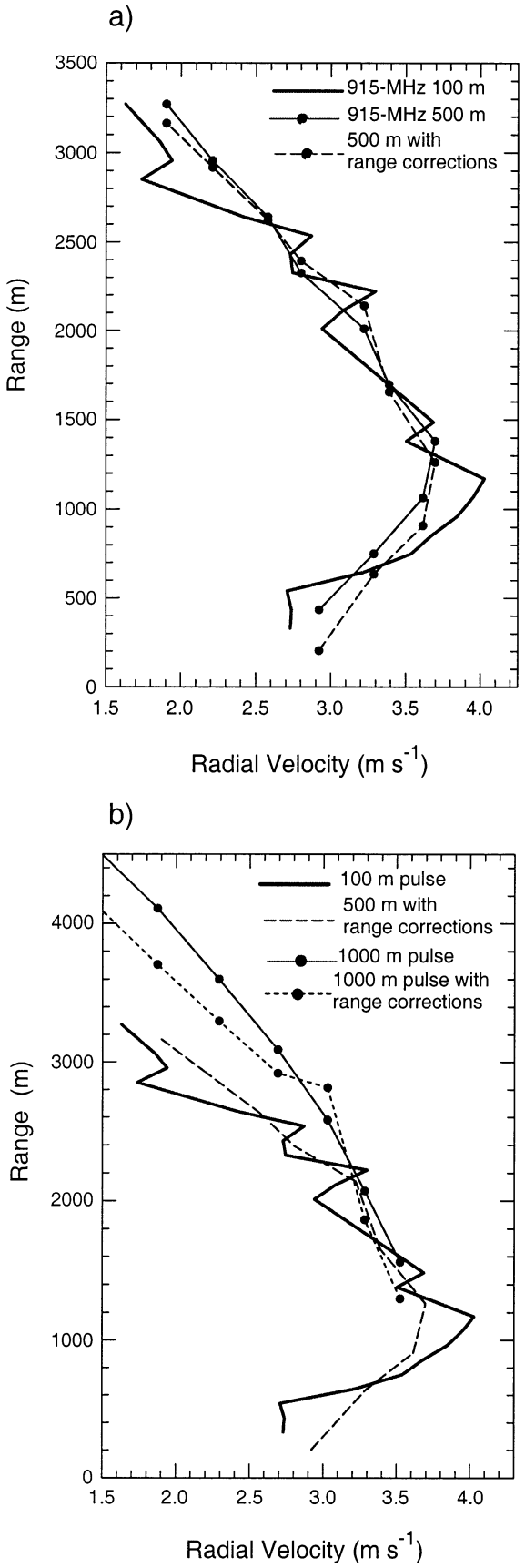

points out the strong variations close to the radar caused by the r^{-2} term.

Figure 12b shows the observed 100-m data and the range-corrected 500-m data from Fig. 12a together with data from the 50-MHz 1000-m pulse length from 1256:44 UTC. The median reflectivity gradient has been applied to the lowest two 50-MHz points. The zenith angles of the two radars' antenna beams differ by 0.5°. By assuming that the vertical wind is zero, the 50-MHz data could be reduced by 3.4% to compensate for the difference in pointing angles. This has not been done on this plot, since the point is clear without the adjustment; the range corrections shift the observed 50-MHz velocities closer to the 100-m pulse length data.

Comparing Fig. 12 with Fig. 1 shows similar issues: the uncorrected 500-m pulse places low-level features like the speed maximum higher than the 100-m pulse; the 500-m profile underestimates velocity maxima relative to the 100-m profile; and the uncorrected 1000-m pulse is consistently above the profiles measured with shorter pulses. The velocity underestimation is caused by the integration over a larger volume and should be accepted as an intrinsic and proper difference. This issue aside, Fig. 12 shows that the range corrections do help to make the velocity profiles more consistent.

7. Synthesis of simulations and radar observations

The radar simulation discussed in section 4 can accept arbitrary reflectivity and velocity profiles as an input. By putting in radar observations, the performance of the simulation with respect to atmospheric observations can be examined. These results demonstrate the validity of the simulation. They also give insight into the way the radar instrument performs and how changes to the operation could be made to improve the measurements.

The profile input to the simulation consists of a set of layers that represents the atmosphere. For each layer, the range, reflectivity, velocity, and layer width are specified. To get an observed reflectivity profile for input to the simulation, Christmas Island 915-MHz, 100-m pulse length radar measurements (shown in Fig. 12) were converted to a reflectivity profile using standard Aeronomy Laboratory software. This software converts the received power observed by the radar to reflectivity using

←

FIG. 12. (a) Radial velocity profiles measured with the Christmas Island 915-MHz wind profiler. All data are from the east antenna beam, with a zenith angle of 76.2°, on 20 Oct 1999. The thick solid line is from the 100-m pulse length at 1256:29 UTC. The thin solid line with the data points is the 500-m pulse length data from 1257:10 UTC. The dashed line is the 500-m data with the range corrections applied. (b) The same 100-m data (thick solid line) and range-corrected 500-m data (dashed line) velocity profiles, together with the 50-MHz 1000-m pulse length data. The 50-MHz data, with a zenith angle of 75.7°, are from 1256:44 UTC. The 50-MHz data as both measured (thin solid line) and with the range-correction applied (dotted line) are shown.

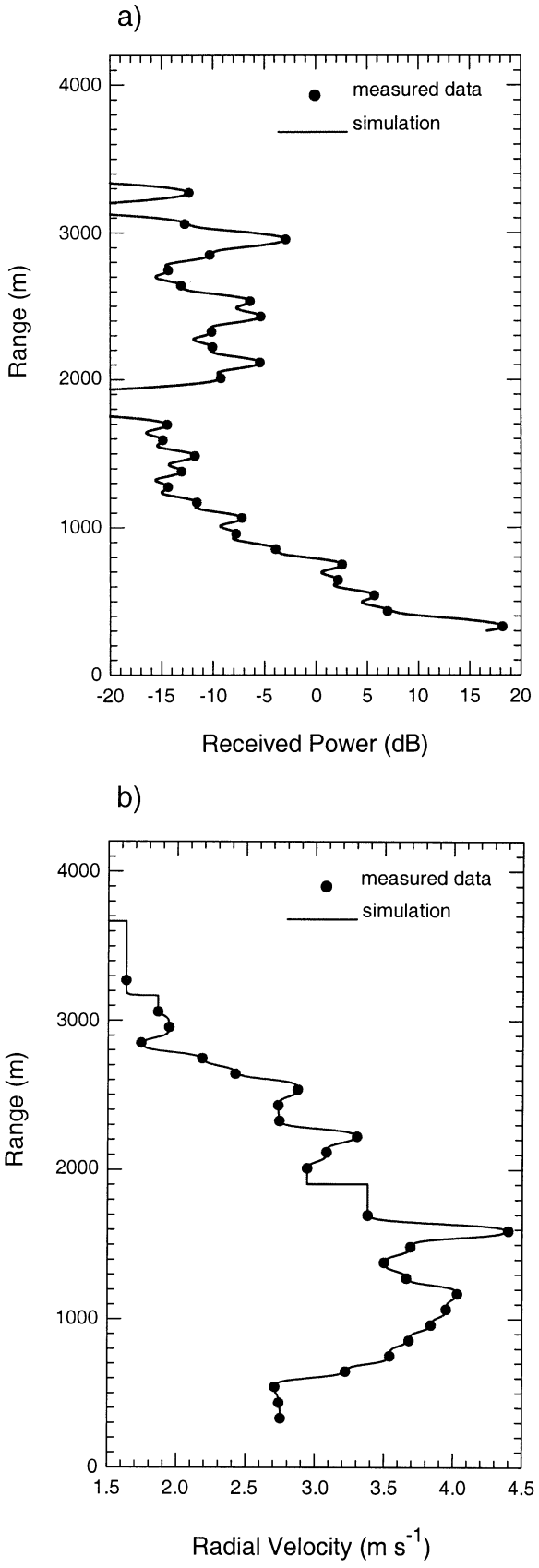

(1). It makes minor corrections to the received power to reduce the effects of the signal-processing methods and outputs range and reflectivity for signals that are above a minimum detectability threshold. This processing is described in detail by the NOAA/Aeronomy Laboratory (1998).

For this portion of the study, the atmospheric profile from the radar was manually edited to correct the velocity of the lowest range, where the wrong velocity was picked by the radar software. The received-power values of the lowest three ranges were corrected to compensate for the pulse coding used to make the radar observations. Since the data are sampled with pulse-length separation and the observations contain no easy way to determine layer thickness, a 1-m layer width was arbitrarily chosen, and is not a reflection of the atmospheric state. This profile starts at 330 m and has ''layers'' every 105 to 3270 m, except at 1800, 1905, and 3165 m, where there was no signal from the radar. The ranges corresponding to the center of the radar's range-weighting function were used for the range values for the input profile to allow for direct comparison with the observations. (The mean range correction based on reflectivity gradients is 3.4 m for this profile, which is negligible for this simulation.)

The first simulation uses a pulse width of 100 m and $B_6\tau$ of 1.0 to show the simulated radar's response to the input profile. Figure 13a shows the received power profiles measured by the radar and generated by the simulation. Figure 13b shows the measured and simulated velocity profiles. The choices of the 1-m layer width and the 100-m pulse length of the simulation combine to make each layer independent of adjacent layers. In Fig. 13 the simulation matches the observed data at the observation points, but away from the observations it shows behavior controlled by the range-weighting function, since no information about the atmosphere is available from the observations. Simulations using other input profiles might match the observations equally well. For instance, representing the peak in the received power at 2500 m by a single layer with more thickness might also be possible, instead of the two layers shown. If this single layer were used, the simulated received power could peak above these two points, instead of having the minima between them.

The simulated received power in Fig. 13a has been scaled to match the measured data at 2955 m. The smallest received-power measurements are close to the minimum-detectable power level of -15.6 dB. There is very good agreement between the simulation and the obser-

←

FIG. 13. Simulation results for a 100-m-long pulse. The input reflectivity and velocity profiles are based on the 1256:29 UTC 20 Oct 1999 100-m pulse length data measured with the Christmas Island 915-MHz wind profiler. (a) The relative received power profile (dB). (b) The velocity profile (m s^{-1}).

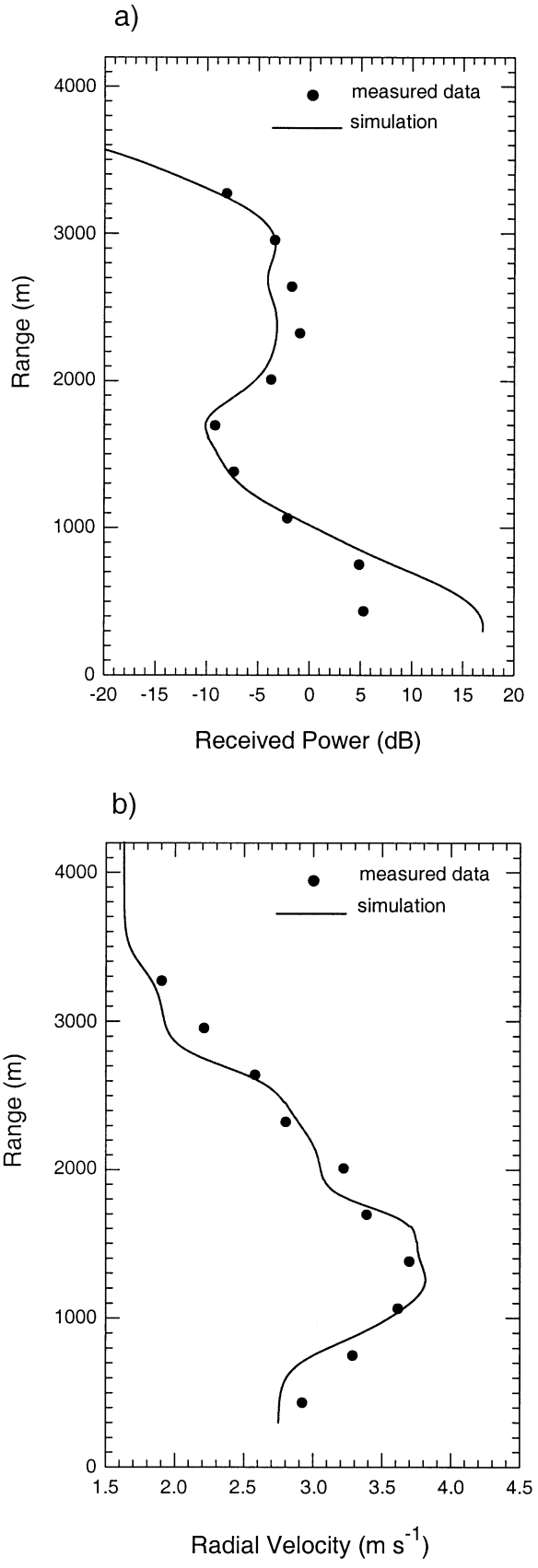

vations at the ranges where the data are specified. Where there are missing data points, the simulation drops hundreds of decibels below the data.

Figure 13b shows the comparison of the radial velocities measured by the radar and estimated by the simulation. The simulation appears as straight lines in areas where there is no data, such as the region around 1900 m, where there is a missing data point. At the points where the 915-MHz radar measured the velocity, the simulation agrees very well with the observations. Note that the velocity maximum near 1600 m was measured at a power level just above the minimum-detectable signal level. Based on typical data quality tests, this point would probably be discarded. For the simulation, leaving it in is acceptable; (4) shows that the velocity is weighted by the reflectivity, and since this data point has a small reflectivity, it will not contribute much to the velocity profile.

Having established that a 100-m pulse length simulation using 100-m observations as an input profile matches the 100-m observations quite well, it is then easy to use this input profile as the input for a simulation of a 500-m pulse length with a $B_6\tau$ of 1.0 and then compare the results with the 915-MHz 500-m observations. Figure 14 shows the comparison of this simulation with the 500-m observations (i.e., the 500-m curve in Fig. 12a). Since the input profile was independently obtained using the 100-m radar data, the simulation results are now a prediction of the 500-m observations.

In Fig. 14a, the received power of the simulation has been scaled to match the 500-m observations at 2955 m. Since the simulated pulse length is now 500 m, the integration is over a larger region and thus includes several layers of the input profile. Therefore, the simulated 500-m profile does not show the extremely small values where there are missing points in the 100-m observations (and simulation). Both the simulation and the radar data show that the received power is well above the −16.6 dB minimum-detectable power level of this system, demonstrating the increased sensitivity of the 500-m pulse length.

The simulation shows that the first data point should have 5 dB more power than the second level, instead of being nearly equal. As has been discussed earlier, it is known that the radar observations of received power are attenuated at this range due to the radar electronics, and 5 dB is not an unreasonable attenuation value. In Fig. 12a, the median reflectivity gradient was used to correct this point, which moved the first 500-m range data down 229 m. If the reflectivity gradient below the second point

←

FIG. 14. Simulation results for a 500-m-long pulse. The input reflectivity and velocity profiles are based on the 1256:29 UTC 20 Oct 1999 100-m pulse length data measured with the Christmas Island 915-MHz wind profiler. The data points shown are from the 1257:10 UTC 20 Oct 1999 500-m pulse length. (a) The relative received power profile (dB). (b) The velocity profile (m s^{-1}).

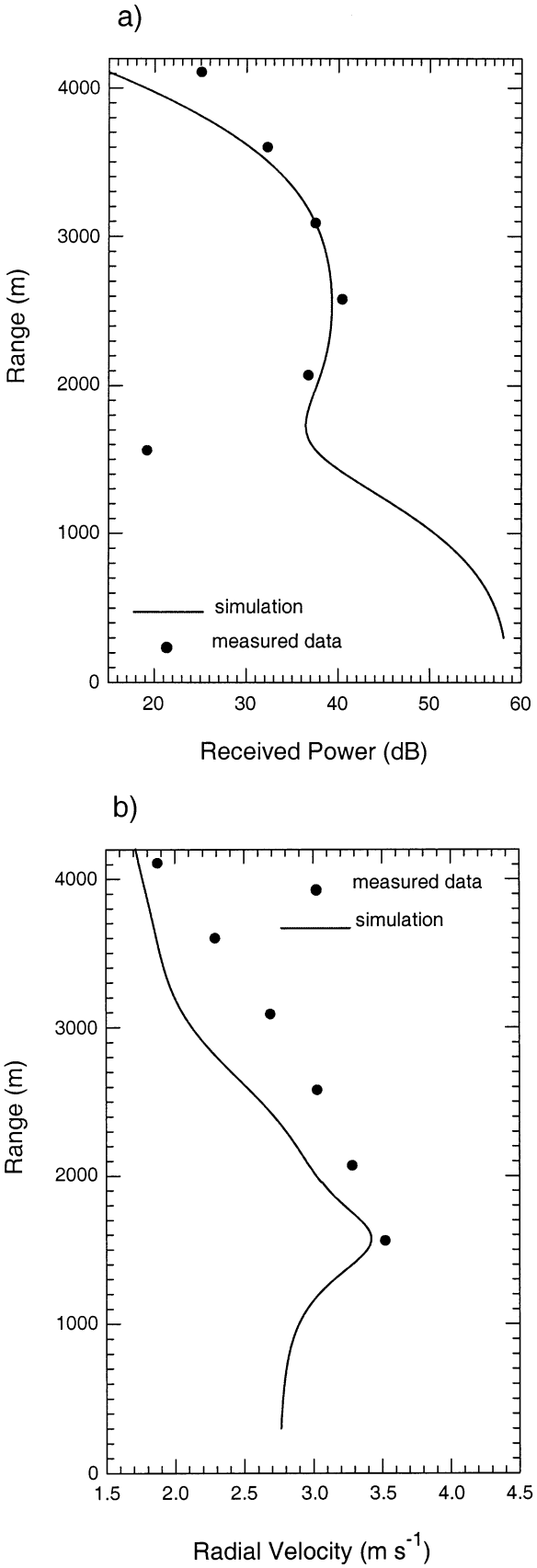

suggested by the simulation (≈ -15 dB km^{-1}) had been used instead of the median value, the range correction applied in Fig. 12a would only increase to 260 m. In this region, close to the radar, most of the correction is due to the r^{-2} term, not the gradient term.

Figure 14b shows the comparison between the observed radial velocity data and the simulation. Figures 14a and 14b show that the input profiles derived from the 100-m data enable the simulation to provide a good prediction of the 500-m data. One of the largest velocity differences is in the first range. One strong possibility for this discrepancy is that the nonlinear response of the radar is shaping the range-weighting function of the radar so that the velocity is more representative of farther ranges. This is a case where possibly the simulation is ''correct'' and the radar is ''wrong,'' and is certainly an area that requires further study.

Figure 15 shows the prediction of the 1000-m 50-MHz radar observations, again based on the 915-MHz 100-m measured values of reflectivity and velocity as the input profile. Figure 15a shows good agreement between the measured signal power and the simulation's predicted signal power. The simulation power has been scaled to match the 50-MHz at 3083 m. The minimum-detectable signal for this system is -11.6 dB, far below any of the values plotted (the 50-MHz radar observed data to 9200 m). With a 1000-m pulse length, the missing 100-m data are not affecting the simulation. It is interesting to note that even though the farthest range in the input velocity profile is 3270 m, the simulation and the data agree well at 3600 m. The recovery problem with the power measured by the first gate is obvious, as the datum at 1557 m is more than 15 dB below the simulation.

Figure 15b shows the measured and predicted velocities. The prediction is not as good as the 500-m prediction, but it is still reasonable. Differences in zenith angle directions of the antenna beams account for about 0.1 m s^{-1} of the 0.3 m s^{-1} difference at 2070 m. The input profile is only defined to 3270 m, and at ranges beyond about 2800 m, the 1000-m pulse data will start to include volumes that are not specified in the input velocity profile, which could account for some of the difference. The 50-MHz data were obtained with a 3° wide antenna beam, while the 915-MHz data comes from a 6° wide antenna beam. In our model we have removed antenna beamwidth effects, but they may be important in this case to fully explain the differences. For this simulation, a $B_6\tau$ of 1.0 was used. We believe

←

FIG. 15. Simulation results for a 1000-m-long pulse are shown. The input reflectivity and velocity profiles are based on the 1256:29 UTC 20 Oct 1999 100-m pulse length data measured with the Christmas Island 915-MHz wind profiler. The data points shown are from the 1256:44 UTC 20 Oct 1999 1000-m long pulse of the Christmas Island 50-MHz radar. (a) The relative received power profile (dB). (b) The velocity profile (m s^{-1}).

this to be appropriate for this radar, but we need to measure this again. As we discussed in section 4, the $B_6\tau$ characterizes the range resolution of the radar. If we are using an incorrect characterization of the radar, then this could also cause some of the differences observed in Fig. 15b.

These simulations using real data illustrate one of main compromises that is made with wind profiling radars: the data that best describe the atmosphere are obtained with short pulses, but the best way to see high in the atmosphere is to use a long pulse.

8. Discussion and future work

We have presented a technique to correct the range assigned to atmospheric echoes displaced from the center of the radar's range-weighting function by gradients in atmospheric reflectivity. Through the use of a simulation, we have examined some details that are not available as part of the radar signals. We have found it difficult to limit the scope of our work, finding many results that raise new questions and will require future research. This section presents some discussion of the technique and some directions for future work.

This work has examined the range-averaging effects of the radar response and how reflectivity gradients can cause the radar response to be not centered on the range-weighting function. This effect is especially obvious in regions of velocity shear in the presence of reflectivity gradients. Green et al. (1979) analyzed this effect as a velocity bias or measurement error in a fixed-range volume. We demonstrated in section 4 that this is a range location error, with the velocity being an average over a volume that may not be centered on the range-weighting function. The magnitude of this location error can be a large fraction of the range resolution (cf. Fig. 11).

a. Remaining issues

The highest priority for our future work is to apply the corrections to many radial profiles and use the results to calculate wind speeds. We wish to show that a large fraction of the discrepancies between the wind profiles in Fig. 1 can be explained by reflectivity-gradient-induced range errors. As work progressed, it became evident that this demonstration was outside the scope of this paper. Several problems must be solved to complete the demonstration. An examination of these problems is helpful in pointing out some limitations and problems with our technique.

The first problem is that the data corrected by the technique do not have constant ranges after correction; interpolation to constant ranges is required for them to be useful. While very basic interpolation schemes are commonly available, we want to be careful to reduce the artifacts that can be introduced by the algorithms. This is especially critical because wind-profiling radars often use low signal-to-noise data, so incomplete data segments are commonplace. We particularly need to examine what happens during the interpolation when data points are noisy or missing.

The second problem is making sure that the echoes are from valid atmospheric targets. The TPPN radars are in places where many problems encountered by wind profilers (e.g., insects and birds, especially migrating flocks) seldom occur. This makes our observations fairly clean and easy to use, but there are still occasions when nonatmospheric targets such as birds and airplanes are observed by the radars. In these instances, the observed gradients are caused by the range-weighting function's response to point targets, and there is no atmosphere-induced range displacement. Except for some of the contents of Table 1, the observations used in this paper have been manually checked, and most nonatmospheric returns were discarded. This needs to be automated for larger datasets.

The third problem is making sure that good reflectivity gradients are computed. As we have noted in several places in this paper, the data from the lowest ranges in several of our radars are not useable for estimating the reflectivity. This is caused both by the radar electronics and by setting the first gate too close to the radar. In some of our radars, the receiver gain is not constant with range, which makes accurate determination of the reflectivity gradient very difficult. To make a good estimate of the reflectivity gradient, the radar system needs to be linear and have constant gain. In addition, the signal processing must preserve the received power of the signal. Some signal processing techniques, such as the statistical averaging method (Merritt 1995) widely used to reduce bird contamination, sacrifice signal power preservation to obtain higher quality radial velocity information. In some instances, such signal-processing techniques are required to obtain useful data, but they make the application of our range-correction technique difficult.

A fourth problem is the characterization and calibration of the radar system. We have assumed that the radar data presented have the system delays properly accounted for so that there are no range biases caused by poor calibration. Also, the $B_6\tau$ product of the radar must be established to accomplish the range correction. Over the last year, we have been double-checking the range calibration and measuring the $B_6\tau$ product of our radars. This problem is very solvable, but it must be addressed since the information required for the range correction is accurate knowledge of r_0 and $B_6\tau$.

We have not tried to hide the very nonlinear part of the problem near the radar where the r^{-2} dominates the integrand. The r^{-2} term is included in our correction technique, but we have not done a detailed examination of the problem close to the radar. This nonlinearity is evident in Figs. 5, 6, and 9. In the region where range is less than three pulse lengths these figures show that very small range measurement errors can cause large reflectivity and range-correction errors. We recommend

being very careful using data below three pulse lengths in range from the radar. Measurements at these ranges are very important to some researchers, so one area of future work will be to determine the sensitivity of these curves to $B_6\tau$. This will help us obtain high quality low-altitude data.

b. Reflectivity in the atmosphere

Section 2 showed that reflectivity gradients exist and can be quite large. We have left the detailed study of the reflectivity gradients and their characterization to future work. We concluded in section 6 that a constant range correction was not justified. A long-term study of reflectivity gradients and their variations might show that the mean gradient at a given height is constant over long periods. Comparisons between radar sites could show a common mean gradient, which would allow the use of a ''standard'' reflectivity profile. This would give a simpler range correction scheme that would improve the measurement accuracy without requiring the correction of each radial profile.

The simulation has been very useful in exploring the reflectivity-gradient problem. As we further refine and explore the technique, we will continue to use the simulation as a tool to understand the underlying processes and the way the radar observes them. One detail mentioned in section 4 is the clipping of the far tail of the integrand when the reflectivity gradient is positive. In the $M = +20$ dB km^{-1} example, Table 2 shows that the peak and first moment are separated by 21 m, while in the $M = -20$ dB km^{-1} case they are only separated by 9 m. This asymmetry in the correction should be examined in more detail and may require a modification of the technique.

c. Radar operations

The simulations give insights into how the radars operate. We have seen in section 4 that taking data at range intervals smaller than the range resolution may give better measurements. Examination of the effects of various $B_6\tau$ values will be helpful in operating the radars to improve data quality. Using simulations like those shown in Figs. 14 and 15 with different pulse lengths and $B_6\tau$ values can help us predict radar performance. These simulations have the advantage of giving results from the same ''atmosphere,'' so that results can be directly compared.

More simulations of radar measurements, such as those in section 7, need to be done to help us understand our observations. Evidently, some of our profilers may be sampling too close to the radar, where the radar response is nonlinear. The simulation and Eqs. (3) and (4) suggest that when the radar response is nonlinear it is hard to know what the radar observations represent, that is, to what volume and range the data apply. These type of studies may suggest modifications to our radars that will provide higher quality data.

We have decided in our work not to do the range correction to the 100-m-long pulse lengths. As shown in Fig. 7, the offsets for the short pulse are small, on the order of 10 m. However, this correction is about 10% of the pulse length and might be important in some wind profiler applications.

d. Other applications

In the course of this work, some possible applications of the reflectivity-gradient information occurred to us. These include better detection of bad data points and edge detection of different atmospheric phenomenon. We examined some of the extreme values of the reflectivity gradients and were able to classify them as caused by birds or airplanes, which are not atmospheric targets. By doing longer-term data characterization, it might be possible to put limits on the possible values of atmospheric reflectivity gradients. These limits could then be used to help automatically remove bad data points. In the UHF radar case, large reflectivity gradients may be related to the top of the boundary layer or to the edges of clouds. Further study could lead to better algorithms for determining boundary layer heights and detecting clouds. In the VHF radar case, the identification of large reflectivity gradients may help locate the tropopause.

This work needs to be applied to RASS. In RASS, sound intensity falls off at up to -40 dB km^{-1}, which has been shown to lead to large errors in the placement of the data. Both Görsdorf and Lehmann (2000) and Angevine and Ecklund (1994) used an integral form of the radar equation, but did not include the r^{-2} in their analysis. Since UHF RASS is used very close to the radar, some nonlinear effects caused by this term may be important.

Another concern is how this work applies to precipitation measurements. Our simulations show that for ranges greater than three pulse lengths, the reflectivity can be estimated with small errors by using (1). In most precipitation events, the reflectivity gradients are small throughout a deep layer, so the range-correction is negligible. However, long-pulse measurements of the brightband in stratiform rain place the freezing level up to 250 m away from collocated short-pulse and radiosonde observations (P. T. May 2001, personal communication). We suspect that since the bright band is an area with high reflectivity gradients, part of the location difference can be explained by reflectivity-gradient-induced displacement.

This work does not address finite antenna beamwidths. This obviously needs to be reexamined, especially in light of the 9° beamwidths used in many 915-MHz profilers. This is a topic that will get complicated very quickly, since the problem becomes a multiple-

integral problem, requiring the use of (2) instead of the single-integral version of the radar equation (3).

9. Conclusions

The assumptions made in applying the ''standard'' radar equation (1) can lead to a variety of problems when applied to wind profilers. These problems include assigning data to the incorrect range and incorrectly estimating the reflectivity observed by the radar. These problems are caused by violation of two assumptions made in the derivation of (1): that the reflectivity is constant throughout the resolution volume, and that the range is large with respect to the pulse length.

Large reflectivity gradients are found over the tropical Pacific. Atmospheric reflectivity gradients of ± 10 dB km^{-1} or larger are common in our observations. Median values from various sites and pulse lengths are similar to each other and to a median atmospheric reflectivity gradient measured by the NBS (Doviak and Zrnić 1993). However, the range of magnitudes is greater at shorter pulse lengths.

A more general radar equation (3) that allows for varying reflectivity and range over the integrated volume has been used to simulate radar response in various situations. The simulations show that for ranges greater than three pulse lengths, (1) is adequate for calculating the reflectivity observed by the radar. At closer ranges, the assumption that the range is much larger than the pulse length is violated, and the errors can be quite large. Data collected within three pulse lengths of the radar should be used with great care.

The radar simulation has led to a better understanding of the range-weighting function and how it affects radar performance. The simulation shows that the range resolution of the radar can be assumed to be constant, but the range assignment depends on the reflectivity. The range resolution of these radars depends on the range-weighting function of the radar. The range-weighting function is a function of the transmitted waveform and the receive-frequency response, and can be characterized using the $B_6\tau$ product. Use of just the transmitted pulse length for the range resolution is not an adequate description of the volume over which the data should be applied. Figure 8 demonstrates the key point of this paper: *the peak of the range-weighting function is not an adequate description of the location of the echoing region when the reflectivity is not constant throughout the pulse volume.*

Simulations using (3) show that the observed gradients in reflectivity can be used to correct the range assignments of the data, reducing the errors caused by the use of (1). We present a technique that uses the observed reflectivity gradients and the $B_6\tau$ product to correct the range location of the data. This range correction of the data appears to improve the velocity profiles, bringing contemporaneous profiles measured with different pulse lengths into closer agreement. Since the range corrections vary from scan to scan, the corrected profiles often have data at different levels from each other. This makes it difficult to calculate horizontal winds and time averages, because the data must first be interpolated to constant ranges in some manner. This has not been done yet, so the original questions about the long-term averages remain to be answered.

The simulation also can help to develop better strategies for using the data, leading to enhanced data quality. These strategies could include improved hardware (e.g., better receive filters), modified operations (different sampling spacings or pulse lengths), and better online software that could make range assignments based on the measured reflectivity gradients. The simulation also points out the need to use the highest-resolution data available, since the location errors are smaller with smaller pulse lengths. In systems that have multiple modes, the highest-resolution data should receive more weight in any combined profiles.

Acknowledgments. The TPPN is supported in part by the Climate Observations element of the NOAA Office of Global Programs and by NSF Grants ATM-9214800 and ATM-94168. Parts of this work were supported by the NASA TRMM Project Office. We would like to thank Wayne Angevine and the anonymous reviewers for their helpful comments on the manuscript.

REFERENCES

Angevine, W. M., and W. L. Ecklund, 1994: Errors in radio acoustic sounding of temperature. *J. Atmos. Oceanic Technol.,* **11,** 937–842.

Carter, D. A., K. S. Gage, W. L. Ecklund, W. M. Angevine, P. E. Johnston, A. C. Riddle, J. Wilson, and C. R. Williams, 1995: Developments in UHF lower tropospheric wind profiling at NOAA's Aeronomy Laboratory. *Radio Sci.,* **30,** 977–1001.

Chadwick, R. B., and M. H. Ackley, 1997: The NOAA profiler network: Experiences and plans. *Extended Abstracts, COST-76, Profiler Workshop 1997,* Vol. 1, Engelberg, Switzerland, European Commision, Directorate-General XII, 51–58.

Doviak, R. J., and D. S. Zrnić, 1993: *Doppler Radar and Weather Observations.* 2d ed. Academic Press, 562 pp.

Fukao, S., M. Inaba, I. Kimura, P. T. May, T. Sato, T. Tsuda, and S. Kato, 1988: A systematic error in MST/ST radar wind measurement induced by a finite range volume effect 2. Numerical considerations. *Radio Sci.,* **23,** 74–82.

Gage, K. S., B. B. Balsley, and W. L. Ecklund, 1990: Wind-profiling Doppler radars for tropical atmospheric research. *Eos, Trans. Amer. Geophys. Union,* **71,** 1851–1854.

——, J. R. McAfee, W. L. Ecklund, D. A. Carter, C. R. Williams, P. E. Johnston, and A. C. Riddle, 1994: The Christmas Island wind profiler: A prototype VHF wind-profiling Doppler radar for the Tropics. *J. Atmos. Oceanic Technol.,* **11,** 22–31.

——, C. R. Williams, P. E. Johnston, and W. L. Ecklund, 2000: Doppler radar profilers as calibration tools for scanning radars. *J. Appl. Meteor.,* **39,** 2209–2222.

Görsdorf, U., and V. Lehmann, 2000: Enhanced accuracy of RASS-measured temperatures due to an improved range correction. *J. Atmos. Oceanic Technol.,* **17,** 406–416.

Green, J. L., K. S. Gage, and T. E. Van Zandt, 1979: Atmospheric measurements by VHF pulsed Doppler radar. *IEEE Trans. Geosci. Electron.,* **GE-17,** 262–280.

Hartten, L. M., and K. S. Gage, 2000: ENSO's impact on the annual

cycle: The view from Galápagos. *Geophys. Res. Lett.*, **27,** 385–388.

Johnston, P. E., S. K. Avery, B. B. Balsley, D. A. Carter, and K. S. Gage, 1997: A trans-Pacific profiler network for tropical dynamics and climate research. Preprints, *22d Conf. on Hurricanes and Tropical Meteorology*, Fort Collins, CO, Amer. Meteor. Soc., 503–504.

Merritt, D. A., 1995: A statistical averaging method for wind profiler Doppler spectra. *J. Atmos. Oceanic Technol.*, **12,** 985–995.

NOAA/Aeronomy Laboratory, cited 1998: Aeronomy Laboratory precipitation data products. [Available online at http://www.al.noaa.gov/WWWHD/pubdocs/TropDyn/tefluna/zipdata/ProfProd.pdf.]

Oakley, T., J. Nash, and M. Turp, 2000: COST76 experience: Networking of European profilers 1997–2000. Preprints, *Fifth Int. Symp. on Tropospheric Profiling: Needs and Technology*, Adelaide, Australia, 41–43.

Probert-Jones, J. R., 1962: The radar equation in meteorology. *Quart. J. Roy. Meteor. Soc.*, **88,** 485–495.

Sloss, P. W., and D. Atlas, 1968: Wind shear and reflectivity gradient effects on Doppler radar spectra. *J. Atmos. Sci.*, **25,** 1080–1089.

Van Zandt, T. E., 2000: A brief history of the development of wind-profiling or MST radars. *Ann. Geophys.*, **18,** 740–749.

Wuertz, D. B., D. E. Wolfe, B. L. Weber, and R. B. Chadwick, 1995: NOAA's Wind Profiler Demonstration Network: An overview of applications and impact on research. NOAA Tech. Memo. ERL ETL-249, NOAA/Environmental Technology Laboratory, Boulder, CO, 29 pp.